

# MULTIFRACTAL DETRENDED FLUCTUATION ANALYSIS AS THE ESTIMATOR OF LONG-RANGE DEPENDENCE\*

DANUTA MAKOWIEC

Institute of Theoretical Physics and Astrophysics, Gdańsk University  
80-952 Gdańsk, Wita Stwosza 57, Poland

ANDRZEJ FULIŃSKI

M. Smoluchowski Institute of Physics, Jagellonian University  
30-059 Kraków, Reymonta 4, Poland

*(Received April 28, 2010)*

Detection method of long-range dependences based on multifractal analysis in time series is proposed. A short description of multifractal analysis and estimator construction (based on Multifractal Detrended Fluctuation Analysis) are given. This method gives accurate results when applied to large scale analysis of fractional Brownian motions (fBm) and describes consistently the mixture of two fBm processes. Finally, this method has been applied to series corresponding  $K^+$  ionic current through the cellular membrane. For times shorter than 1 sec, a similarity between ionic  $K^+$  current and the mixture of two antipersistent processes has been found with self-similarity parameter of this mixture less than 0.30.

PACS numbers: 05.45.Tp, 05.40.Fb, 02.70.Rr, 87.16.Uv

## 1. Introduction

Natural systems signals need special tools to treat properly their non-stationarity and multiscale organization. Especially, the presence of scaling in time series implies that the usual intuitive search techniques, such as *e.g.* characteristic scale, must be replaced by evidencing relations between scales. The relation between the statistical self-similarity of fractional Brownian motions (fBm) and their increment processes: fractional Gaussian noises (fGn) establishes a starting point for considerations of links between long-range dependencies and scaling [1]. The multifractal formalism is one among

---

\* Presented at the XXII Marian Smoluchowski Symposium on Statistical Physics, Zakopane, Poland, September 12–17, 2009.

many techniques to find self-similarity exponents. The so-called asymptotically second-order self-similarity caused by aggregation makes this formalism widely applicable [2–7].

A method based on well known multifractal properties of the standard synthetic signals such as  $fGn_H$ ,  $fBm_H$  and integrated  $fBm_H$  is used to avoid complaints about reliability and misleadings received otherwise [8]. Namely, point spectra at  $(0, 1)$ ,  $(H, 1)$  and  $(1 + H, 1)$  which are expected in the case of  $fGn_H$ ,  $fBm_H$  and integrated  $fBm_H$ , respectively, are used for discrimination of the type of an unknown signal. Our paper consistently uses simultaneous analysis of the three related signals: an original signal, the signal of increments and the integrated signal to decrease traps of the intrinsic peculiarity in the multifractal analysis.

Spectra received for two types of  $fBm_H$  mixtures: a random mixture of  $fBm_{H1}$  and  $fBm_{H2}$ , and by regular switches between  $fBm_{H1}$  and  $fBm_{H2}$  will be discussed in details. It will be shown that our method is effective in detection of the intrinsic organization in a random mixture. In the case of regular switches between two  $fBm$  signals non-homogeneous scaling features are observed — scaling properties in fine scales are completely different from scaling properties on large scales. The crossover point is related to the switching interval. Hence Stoev's *et al.* [4] idea that a multifractal spectrum is not the only signal representation received from the multifractal approach obtains a practical shape — the important information can be extracted from changes of the scaling. Moreover, unhidden in this way, time scales can be then related to particular phenomena which form a signal [3]. Such approach was successfully applied to series representing time intervals between subsequent heart contractions [6, 7].

Section 2 gives some details of the method necessary for still not standardized multifractal tools used. A construction of the estimator (based on Multifractal Detrended Fluctuation Analysis) is given as well. In Section 3 the multifractal protocol to discover monofractality is proposed. Section 4 reports results found for mixtures of fractional Brownian motions. Finally, the method is applied to the series of values of potassium ions' currents passing through the biological channel.

## 2. Long-range dependence versus multifractal analysis

### 2.1. Long-range dependence

The rigid autocorrelation structure of fractional Gaussian noise —  $fGn_H$ , implies that the integrated process — fractional Brownian motion  $fBm_H$ , is self-similar with the self-similarity parameter  $H$ .  $fBm_H$ s are the unique self-similar processes with the self-similarity index  $H \in (0, 1)$ , and with stationary Gaussian increments [9].

The correlation function of  $fGn_H$  can be approximated by the power-law function:

$$r_{fGn_H}(k) \sim H(2H - 1)k^{2H-2} \quad (1)$$

for large  $k$ . Notice that the correlation vanishes when  $H = \frac{1}{2}$  or  $H \rightarrow 0$ . The case  $H = \frac{1}{2}$  describes the Brownian walk ( $= fBm_{1/2}$ ) and the corresponding Brownian noise ( $= fGn_{1/2}$ ) is not correlated. If  $H > \frac{1}{2}$  then the decay of the correlation is so slow that  $r_{fGn_H}(k)$  is not summable over  $k$ . A corresponding process  $fGn_H$  has the long range dependence (LRD). If  $H < \frac{1}{2}$  (the correlation function takes negative values) then a signal is anticorrelated.

Long range dependence (LRD), which was discovered in many different real signals, see *e.g.*, [1] for examples, is thought to be an important feature of stationary signals. Therefore, the presence of LRD has inspired a weaker concept of self-similarity, namely, in terms of second-order statistics only. It appears that LRD can be equivalently characterized by properties of the aggregated processes.

Formally, let  $X(n)$  be a sample path of some process  $X$ . Then it can be shown [10] that the process  $X$  and the averaged process  $X^{(m)}$ :

$$X^{(m)}(k) = \frac{1}{m} \sum_{n=km}^{(k+1)m-1} X(n) \quad (2)$$

have both identical correlation structure and that

$$r_X(k) \sim k^{2H-2} \quad (3)$$

is equivalent to

$$\text{var} [X^{(1)}(k)] \approx m^{2-2H} \text{var} [X^{(m)}(k)] \quad (4)$$

which implies that the correlation exponent  $H$  for the signal  $X$  can be equivalently estimated from the scaling properties of the variance of the aggregated processes  $X^{(m)}$ . Therefore it is said that  $X$  is asymptotically second-order self-similar with self-similarity parameter  $H$ .

Estimates of LRD from plots of variance *vs.* time are known to be unreliable [11]. Alternatively LRD can be measured through spectral properties because (3) is equivalent to the power-law behavior of its Fourier transform, *i.e.*, to the power spectrum of a signal. In the next section the method of estimation of LRD based on multifractal formalism will be investigated.

2.2. Multifractal analysis

The mathematical meaning of multifractality arises from an idea of the pointwise regularity of a continuous function  $X(t)$ , see, *e.g.*, [9, 12, 13]. Multifractal analysis provides the description of the fractal structure of subsets of the domain of  $X(t)$  selected by fractional singularities. Formally, the multifractal spectrum  $h \rightarrow D(h)$  (the aim of the multifractal analysis) displays a decomposition of the domain of  $X(t)$  according to  $X(t)$ 's singularity exponents: it assigns a Hausdorff dimension  $D(h)$  to the domain subset which collects  $t$  points where the singularity exponent is equal to  $h$  [9].

Let  $\{X(i)\}_{i=1,2,\dots}$  be a discrete approximation of a sample path of some stochastic process  $X(t)$ . Let the series  $\{X(i)\}$  be divided into boxes consisting of  $n$  points. Any quantity  $R_X^{(n)}(k)$  which describes some property of a signal in a  $k$ -th box is called a *multiresolution quantity*. It is said that  $X$  possesses scaling properties if the partition function  $F(n, q)$  — the average of  $q$  moments of a given multiresolution quantity, depends on a scale  $n$  in the power-law form, namely:

$$F(n, q) = \frac{1}{K} \sum_{k=1}^K \left| R_X^{(n)}(k) \right|^q \propto |n|^{\tau(q)}, \tag{5}$$

where  $\tau(q)$  is called the scaling exponent function and  $q$  takes real values. The positive  $q$  describes wild parts of a signal whereas the negative  $qs$  collect properties of smooth parts of a signal. The multifractal spectrum  $(h, D(h))$  is obtained by the Legendre transform applied to the scaling exponent function  $(q, \tau(q))$ :

$$h = \frac{d\tau(q)}{dq}, \quad D(h) = qh - \tau(q). \tag{6}$$

The theory gives freedom in choosing the form of the multiresolution quantity — several statistics have been considered as  $R$  [2, 9, 12, 13] and still new propositions appear, see, *e.g.*, [14]. A lot of simulations (see *e.g.* [2, 4, 6, 7, 13, 15]) were performed to validate numerically different procedures. A popular method is called Multifractal Detrended Fluctuation Analysis (MDFA) [13].

The MDFA method estimates departures of a signal path points  $X(i)$  from a local polynomial trend:

$$R_{X, P_m^k}^{(n)}(k) = \left( \sum_{i=kn+1}^{(k+1)n} \left[ X(i) - P_m^k(i) \right]^2 \right)^{1/2}, \tag{7}$$

where  $P_m^k$  is the best polynomial approximation of the order of  $m$  found for the points from  $k$ -th box. The partition function  $F(n, q)$  is given as

$$F(n, q) = \sum_{k=1}^K \left( R_{X, P_m^k}^{(n)}(k) \right)^q . \tag{8}$$

Hence the scaling of  $F(n, q)$  determines the scaling exponent function  $\tau(q)$ , and then the multifractal spectrum  $h \rightarrow D(h)$ . Notice that proposed above the MDFA method is slightly different from the original one [13] where so-called profiles of a signal, namely an integrated signal, are considered. The MDFA method has been found as satisfactory, accurate, and weakly dependent on the method parameters, while it was tested on synthetic data [5, 13, 15]. In the following, we use the square detrending *i.e.*,  $m = 2$  and the software packets of Physionet [16] to calculate (8).

### 2.3. LRD from multifractal analysis

The multifractal scaling exponent  $\tau(2)$  which corresponds to the second moment of the partition function, measures also the power-law behavior of the second-order statistics, hence describes LRD. However, LRD is defined in the limit of large scales while multifractal analysis is formulated in the limit of fine scales. Therefore the limit exponents: for fine scales and for large scales, are exactly the same only if the scaling is the same on all scales. So, when the scaling in fine scales differs from the scaling in large scales then these two approaches provide different answers [9].

It can be proved [9] that if a process  $X$  has zero-mean increments then the correlation function of increments is determined by

$$H = \frac{\tau(2) + 1}{2} . \tag{9}$$

The self-similar processes with stationary increments have the simplest multifractal spectra. A sample path  $\text{fBm}_H$  has everywhere a local singularity exponent equal to  $H$  what leads to the multifractal spectrum concentrated in a point  $(H, 1)$ . It denotes the corresponding signal of increments:  $\text{fGn}_H$  has LRD which is described by  $H$ . However  $\text{fGn}_H$  itself has the multifractal spectrum in a point  $(0, 1)$  because there is no LRD between increments of  $\text{fGn}_H$ . The multifractal spectrum of a process of integrated values of  $\text{fBm}_H(i)$ :

$$\text{fBm}_H^{\text{int}}(k) = \sum_{i=0, \dots, k} \text{fBm}_H(i)$$

is also a point which is located in  $(H^{\text{int}} = 1 + H, 1)$ . The distance between the spectrum for the original signal  $\text{fBm}_H$  and integrated signal  $\text{fBm}_H^{\text{int}}$  is equal to 1 what implies strong deterministic-like dependence in the incremental process of  $\text{fBm}_H^{\text{int}}$  *i.e.*, in  $\text{fBm}_H$  itself.

Formula (9) holds for all self-similar processes with stationary zero-mean increments, therefore it holds for Lévy motions, too. The Lévy stable motion  $L_\alpha$  is the self-similar, symmetrical  $\alpha$ -stable process with stationary and independent increments [9]. The self-similarity exponent  $H$  of  $L_\alpha$  is related to the stability index  $\alpha$  by a relation  $\alpha = 1/H$ . The stability index describes the decay of the distribution tails, namely the tail decay with a power-law with the exponent  $\alpha$  (such a distribution is called  $\alpha$ -stable distribution). Since  $L_\alpha$  has independent increments (and so  $L_\alpha$  generalizes the fractional Brownian motion in the case when  $H = \frac{1}{2}$ ) therefore, it does not provide a modeling of LRD. The multifractal spectrum of  $L_\alpha$  consists of two points:  $(0, 0)$  and  $(1/\alpha, 1)$ . In Fig. 1 we plot an example of the multifractal spectrum received for  $L_{1.5}$  and its increments. The spectra are similar but shifted by  $1/2$  in  $h$  values. It appears that correlations and non-stationarity of a noise with  $\alpha$ -stable distribution do not influence the multifractal spectrum of the corresponding Lévy process [17].

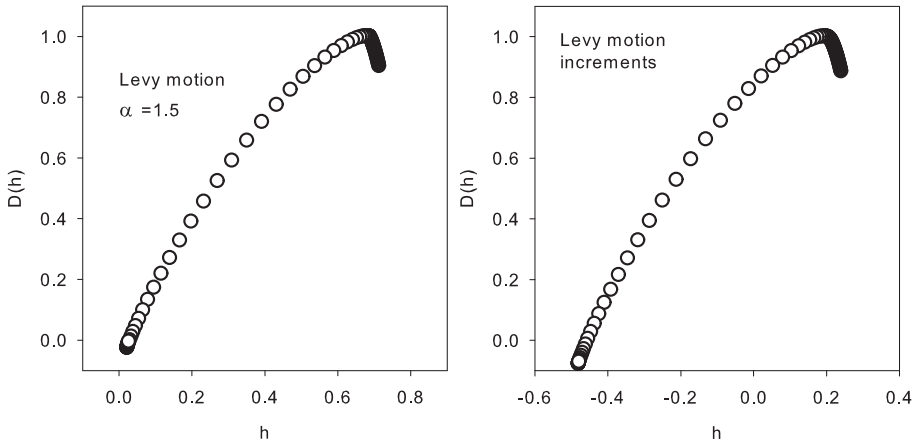


Fig. 1. Multifractal spectrum for Lévy motion  $L_{1.5}$  (left), and for corresponding Lévy noise (right) received from the MDFA partition function (8). Notice that the multifractal spectra, when considered numerically and from limited data sets, are not the two points but they consists of all values between the two points.

Detrended Fluctuation Analysis — the base on which the MDFA method has been derived, is known to be a reliable tool to quantify accurately correlations in noisy signals embedded in polynomial trends [18]. However, if it is not known whether a given time series has LRD, it is advised to compare the results with other methods [5].

### 3. Protocol to estimate LRD by multifractal tools

There are two main reasons for multifractality observed in time series: one related to the broad distribution (like in Lévy motions) and second due to LRD [5]. The practical use of multifractal formalism suffers from numerical difficulties so it happens that results are misinterpreted [2–5, 19]. The basic misleading is related to the fact that the scaling found numerically — from log–log plots of (8), is not uniform in all scales but changes when the box size  $n$  is changed. Even in the simplest case of fBm $_H$  the effect is noticeable (see Appendix A for explanation).

In the case of fBm $_H$  signals the relation between LRD and multifractality is the most straightforward and therefore, the quality of the MDFA method can be evaluated by practical tests [6, 7]. Tests were performed on 50 samples (consisting of 25000 points) of each process fBm $_H$  with  $H = 0.1, 0.2, \dots, 0.9$ . (Signals were prepared by tsfBm packet [20].) Properties of multifractal spectra obtained on large scales by the MDFA method are collected in Fig. 13, right column in Appendix A. Following them we claim that MDFA gives satisfactory and consistent results for fBm $_H$  signals, however, only if the multifractal analysis is performed on large scales, *i.e.*, when  $\log n > 2$ . Finally we propose the following protocol to validate the MDFA method as the self-similarity estimator:

*Protocol for monofractal indices by multifractal tools:*

- (A) If for each  $q$  a linear approximation for  $\log F(n, q)$  vs.  $\log n$  dependence is found over the same range of scales and the Pearson correlation error  $r^2 > 0.98$ , then the scaling exponents  $\tau(q)$  are considered as representatives for the underlying scaling phenomenon.
- (B) If the width of the multifractal spectrum is smaller than 0.05 then the spectrum is assumed as a monofractal.  
 If a spectrum has a nonsymmetric shape with one wing larger than the other one then ignore the larger wing, and estimate the *width* as the shorter wing doubled, see Appendix B.  
 If a shape is not a parabola-type then one should apply symmetric conversions (reflection mainly) which transform the spectral points into a concave curve.
- (C) If the maximum of the multifractal spectrum is the only spectrum accumulation point  $h_{\text{acc}}$ , see Appendix C, then the spectrum is assumed as a monofractal.  
 The spectrum accumulation points must be determined by observation distributions of  $h_i$  in different  $q$ -intervals. If the spectrum is multivalued, we propose to consider  $q$  interval which corresponds to the convex part of  $\tau(q)$ , namely, the part where  $h(q)$  is a strictly monotonic function of  $q$ .

- (D) If the exponent  $H$  estimated directly from  $\tau(2)$  following (9) is equal to  $h_{acc}$  then the spectrum is assumed as a monofractal.
- (E) If the multifractal spectrum of the integrated signal satisfies (A)–(D) and is described by  $1 + h_{acc}$  then the spectrum of the original signal is assumed as a monofractal.

When all above conditions are satisfied then a given signal can be claimed as a monofractal.

#### 4. Detection of monofractality in switched fBm signals

Let us apply our protocol to description of the multifractality of the mixture of two different fBm series. As an example, we consider a signal received by switching at random from a sample path of fBm<sub>0.1</sub> to a sample path of fBm<sub>0.2</sub>. The steps of our analysis are presented in Fig. 2.

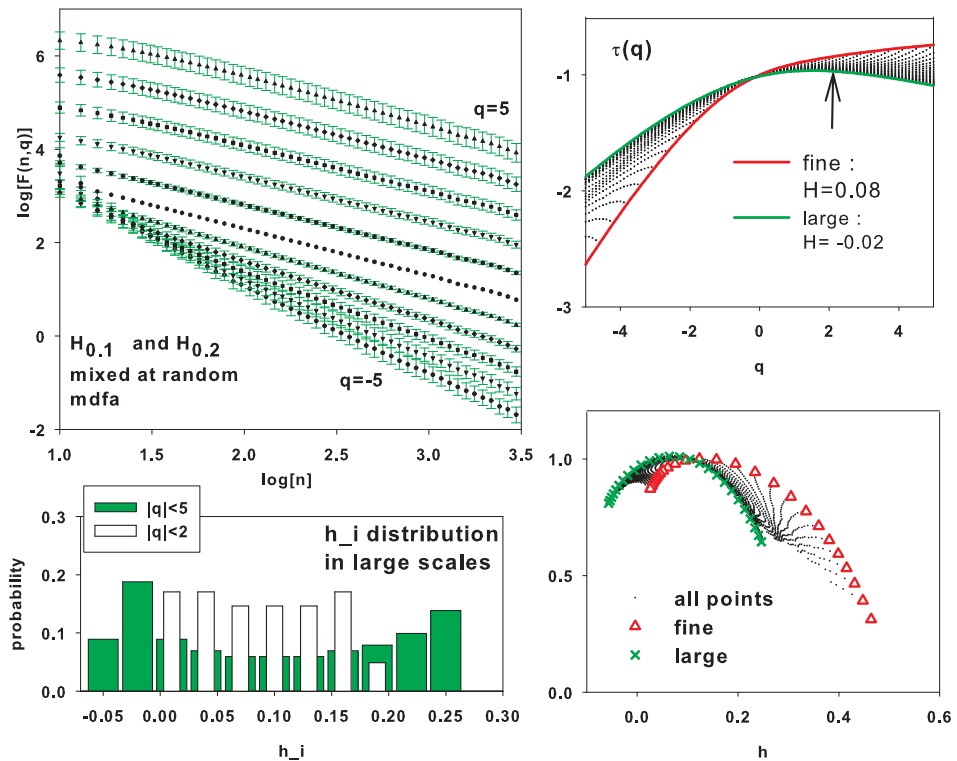


Fig. 2. Left top: Means of partition functions found for 30 independent samples of fBm<sub>0.1</sub> and fBm<sub>0.2</sub> random mixture, together with the std errors of means. Right top: Scaling exponent functions  $\tau(q)$  formed according to the partition functions. Right bottom: Multifractal spectra, respectively. Left bottom: Distributions of  $h_i$ .

The mean partition function of the random mixture of  $fBm_{0.1}$  and  $fBm_{0.2}$  (found from 30 independent runs) weakly depends on a scale, see left top panel in Fig. 2. However, by using a sliding window (consisting of 40 points) one can extract a family of scaling exponent functions  $\tau(q)$ s and calculate the corresponding multifractal spectra. It is evident that there is a difference in results when different scales are taken into account. To extract LRD properly, we concentrate on large scales, *i.e.*, when  $n > 500$ . Additionally, the partition functions have the smallest variability if  $|q| < 2$ . Therefore, we limit our analysis to this  $q$ -interval. An example is shown in Fig. 2, left bottom. To retrieve the description of LRD via second-order self-similarity, we calculate  $H$  from  $\tau(2)$ .

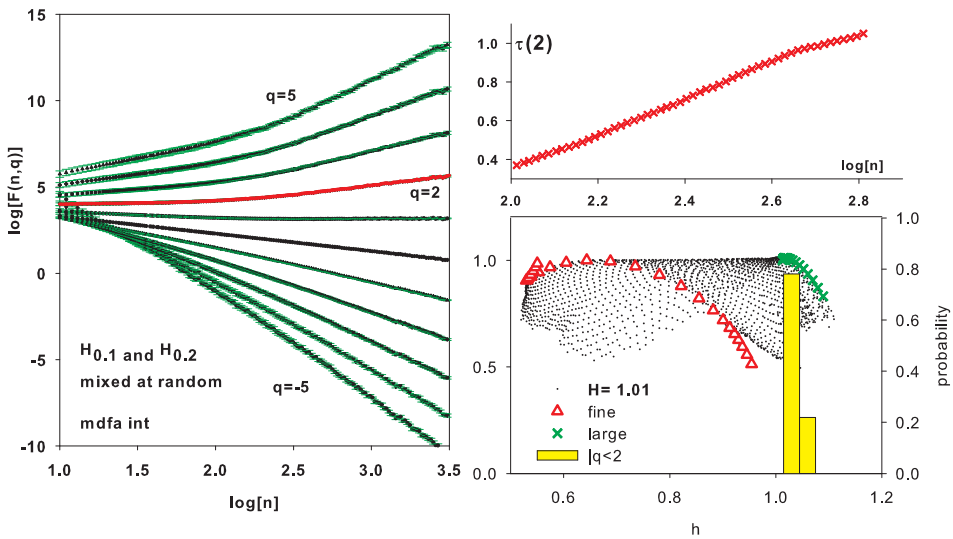


Fig. 3. Left: Means of the partition functions found for 30 different samples of  $fBm_{0.1}$  and  $fBm_{0.2}$  integrated together with std-errors of means. Right top: Dependence of  $\tau(2)$  on scales (the middle of a window of 40 subsequent points is assigned) where scaling is performed. Right bottom: Multifractal spectra and distributions of  $h_i$ .

In this particular case when the mixture is made of  $fBm_{0.1}$  and  $fBm_{0.2}$ , the distribution of accumulation points is roughly uniform for  $0 \leq h_i \leq 0.15$  — no accumulation point can be marked out, and the spectrum width is far from a point-type. The exponent  $H$ , calculated from  $\tau(2)$ , is  $H = -0.02$  what agrees with the left limit of the spectrum. Moreover,  $D(0) \gg 0$ . All these properties lead to the conclusion that correlations among increments are not present. Nevertheless one can test whether the signals are similar to a correlated noise if the analysis is performed on integrated series. Integrated

signals provide an evident dependence of the partition function on a scale in which the scaling is performed, see Fig. 3, left. Because of this dependence the value of  $\tau(2)$  changes significantly when scaling moves from fine to large scales. However, on large scales only, a narrow multifractal spectrum concentrated at  $h_{\text{acc}} = 1.05$  and with  $H = 1.01$  for LRD (what approximates 1.0 accurately) is found see Fig. 3, right bottom. According to our protocol the noisy signals, which are studied, are driven deterministically.

In Fig. 4, left column, we present the multifractal spectra and properties of distributions of  $h_i$  for random mixtures of two signals  $\text{fBm}_{H_1}$  and  $\text{fBm}_{H_2}$  for different  $H_1$  and  $H_2$ . Results can be summarized as follows. The spectrum of a random mixture of  $\text{fBm}_{H_1}$  and  $\text{fBm}_{H_2}$  concentrates in two points. The first point is  $h'_{\text{acc}} = 0$  and  $D(0) = 1$  what significantly discerns the considered signal from a Lévy motion. This spectrum accumulation point comes from  $q > 0$  what also results in  $H = 0$ . The localization of the second point varies from a sample to a sample because its value comes from  $q < 0$  what is a numerically sensitive part of a partition function. The most probable value for the second spectrum accumulation point is  $h''_{\text{acc}} = \max\{H_1, H_2\}$  with  $D(h''_{\text{acc}}) = 0$ . Hence the smoother path of the random mixture is detected by negative moments. Following our experiments we claim that

$$\tau(-2) = -\max\{H_1, H_2\} - 1. \quad (10)$$

At labels in Fig. 4 we give both: the values of  $H$  from the LRD statistics and  $\tau(-2)$  to support the above observation.

The integrated signals provide also a two-point-type multifractal spectra, see Fig. 4, right column. If there is a large difference between  $H_1$  and  $H_2$ , or when both signals are persistent, then the first point is  $(1/2, 1)$ , as expected from randomness of increments. The second point is approximately at  $(1 + \max\{H_1, H_2\}, 0)$  what is expected from the discovered structure in the direct signals.

We have to emphasize that our conclusions are derived from studies of averages of partition functions, and therefore, when an individual run is observed then a different answer can be easily found.

Finally, let us check the influence of regular switches between the two paths — let a signal be generated by switching from a path of  $\text{fBm}_{H_1}$  to a path of  $\text{fBm}_{H_2}$  after each step. In particular, we study  $\text{fBm}_{0,1}$  switched to  $\text{fBm}_{0,2}$ . In Figs. 5 and 6 multifractal analysis is presented as an example.

It appears that the multifractal picture of regularly switched  $\text{fBm}$  paths is similar to a picture obtained for a random mixture. However, the results received for the corresponding integrated signals are significantly different. The partition functions exhibit the evident crossover property. The cross point depends on the value of  $H$  of participating signals, but approximately, the change occurs on scales of hundreds. As a consequence, the fine and

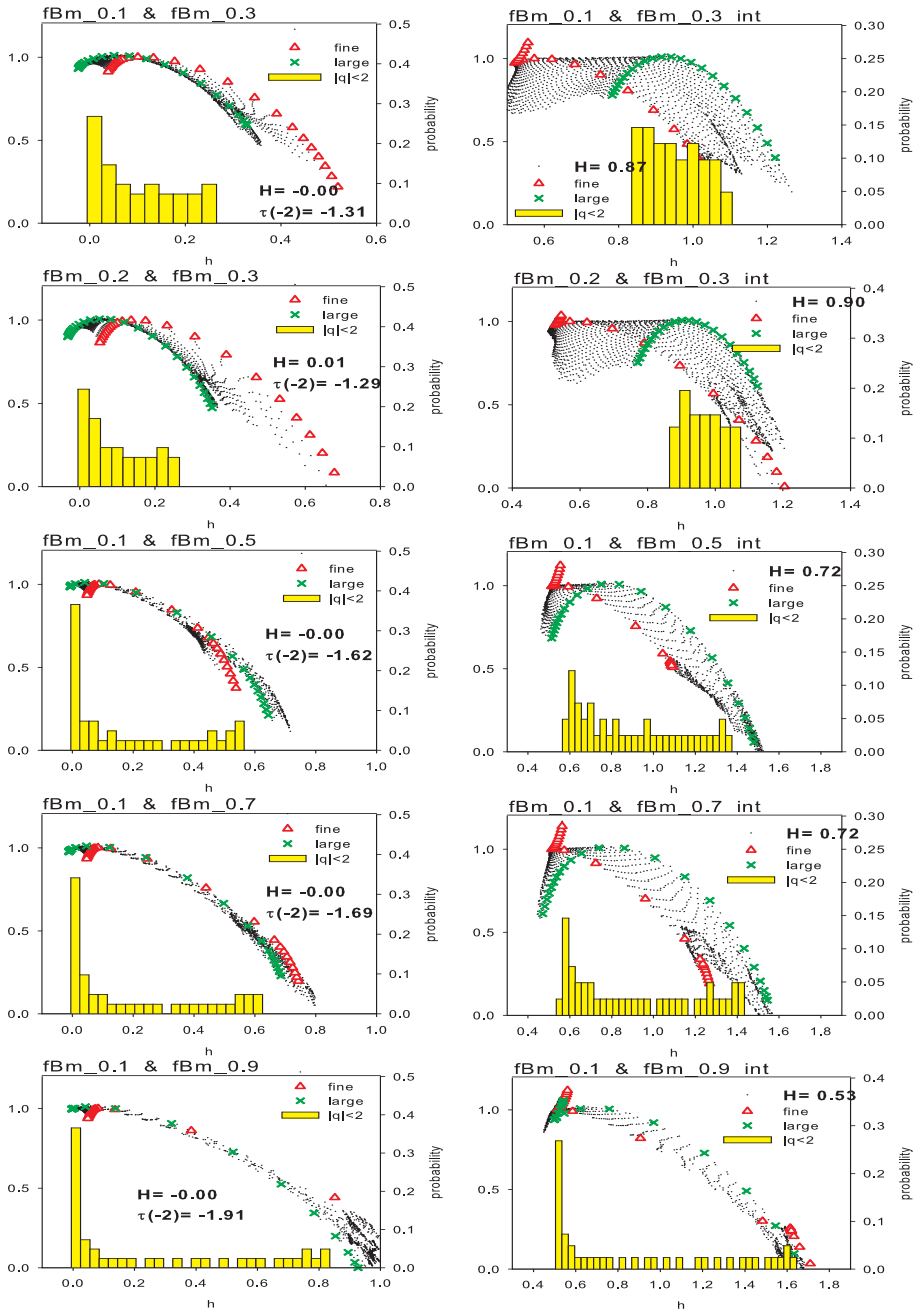


Fig. 4. Results of multifractal analysis and  $H$  for LRD received for different random mixtures of two fBm signals.

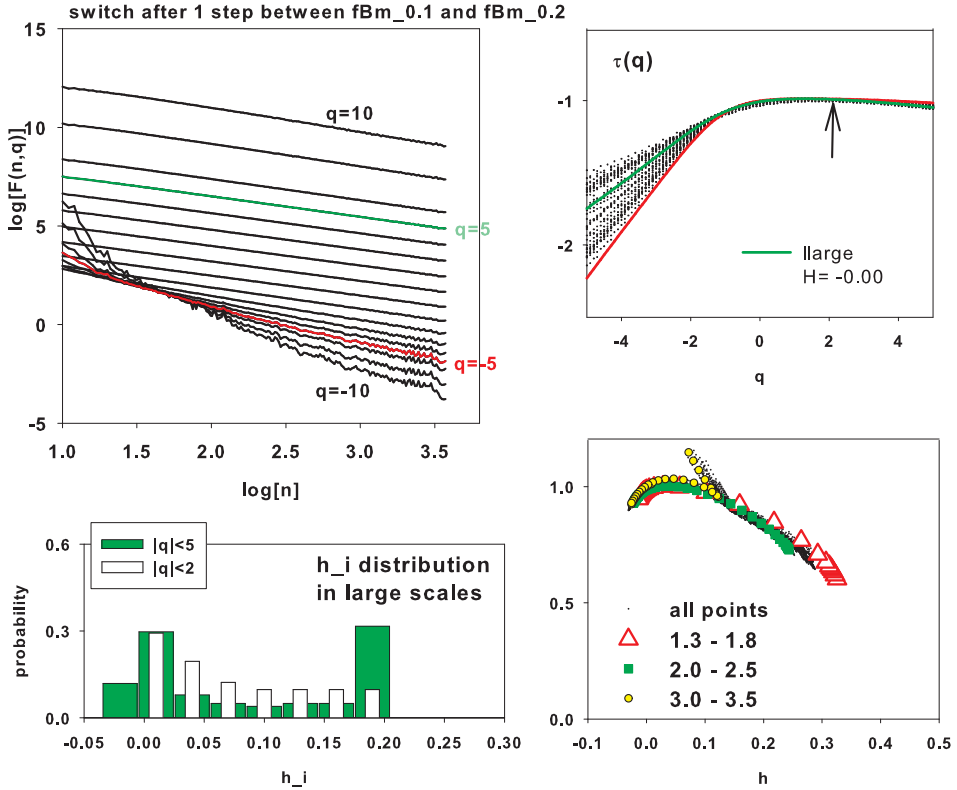


Fig. 5. Left top: Partition function for a signal received when a path of  $fBm_{0.1}$  is switched to a path of  $fBm_{0.2}$  and back after each step. Right top: Scaling exponent functions  $\tau(q)$  formed according to the partition function. Right bottom: Multifractal spectra. Left bottom: Distributions of  $h_i$ .

large scales estimates are sharply different from each other. The fine scales always lead to  $h_{acc} = 0$ , but the large scales spectra recall ones received for a random mixture.

The emergence of the crossover property in partition functions is amplified when regular switches between paths occur more rarely. In Fig. 7 such partitions functions are shown. A signal consists of subsequent hundred points of  $fBm_{0.1}$  switched then to hundred points of  $fBm_{0.2}$  and so on. The change in scaling properties is present in both partition functions: the direct signal and integrated signal. The really rapid change is observed for  $q$ s positive. The crossover point is about the same in both cases and it occurs at scales of hundreds. So by discovering a switch in scaling properties of partition functions one can learn about the type of a signal mixture — whether is regular or random?

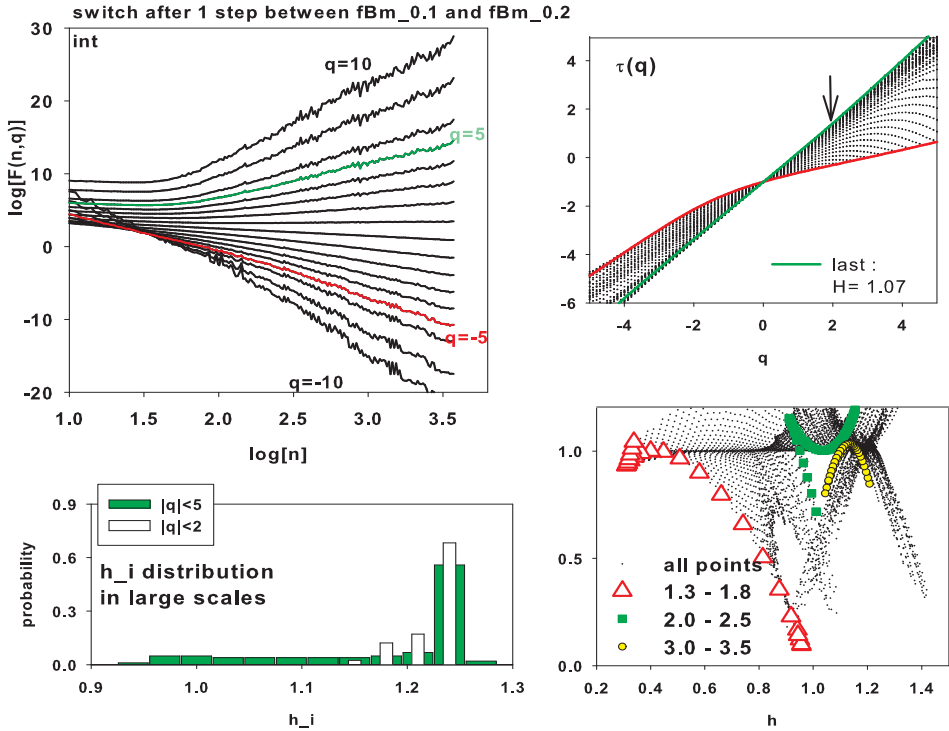


Fig. 6. Description to plots is the same as in Fig. 5 but refers to the integrated signal.

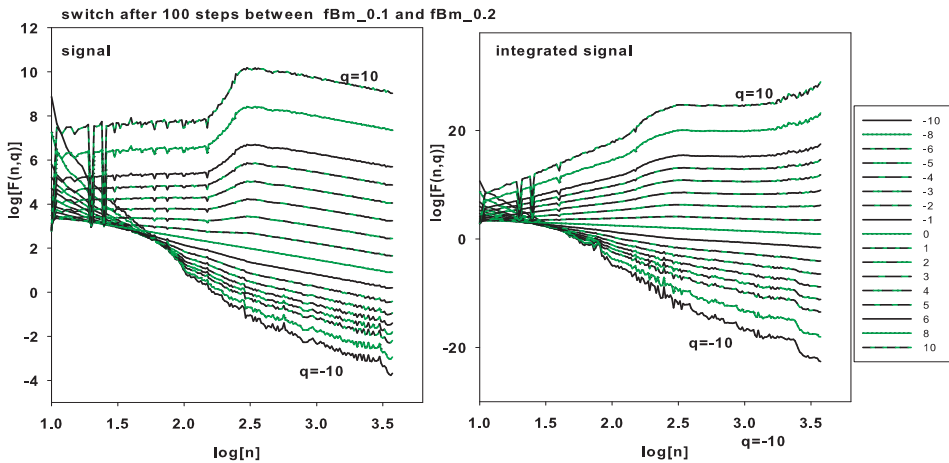


Fig. 7. Partition functions for signals received when paths of  $fBm_{0.1}$  and  $fBm_{0.2}$  are switched to each other after every 100 steps.

## 5. Biological currents series

This section presents a detailed analysis of potassium ions' currents passing through the biological channel. The channel consists of four protein sub-units which create an inverted cone with charged entrances [21, 22]. These data were extensively discussed in several papers [24–29] and their stochastic properties are known. Adult locust (*Schistocerca gregaria*) extensor tibiae muscle fibers with cell attaches patches were the sources of these signals [23].

### 5.1. General characteristics of the signal

The data set consists of 250 000 values corresponding to the channel currents  $I(t)$  excited at 60 mV and measured at  $\delta t = 0.0001$  s time intervals. The minimum and maximum currents are:  $I_{\min} = 0.24$  and  $I_{\max} = 20.46$  pA, respectively. The time dependence of this signal, normalized to unit interval (called BION):

$$i(t) = [I(t) - I_{\min}] / [I_{\max} - I_{\min}], \quad i(t) \in [0, 1], \quad (11)$$

is shown in Fig. 8.

The whole signal is bimodal (*cf.* Fig. 9 below), with peaks at about 3.1 and 13.0 pA [24, 26–29]. The distribution of transitions between both modes (low-value and high-value currents) is bimodal and shows roughly the same location of peaks [24]. Moreover, the signal is non-Markovian [24–28], and its power spectrum  $S(f)$  is of the flicker-noise type ( $S(f) \sim f^{-B}$ ), with the exponent  $B = 1.1 \pm 0.1$  [25, 26].

The distributions of currents from biological channels are usually represented by linear combinations of several Gaussian functions. This is certainly possible: a linear combination of sufficiently many Gaussians is able to reproduce any function. However, we found that much better fit of the BION data distribution  $P(i)$  can be obtained as a linear combination of two, appropriately scaled and shifted, non-Gaussian, heavy-tailed asymmetrical  $\alpha$ -stable distributions:

$$P(i) = 0.80 P_{\text{st}}(1.58, 0.75) + 0.20 P_{\text{st}}(0.75, -0.8), \quad (12)$$

where  $P_{\text{st}}(\alpha, \beta)$  denotes the  $\alpha$ -stable distribution of the considered quantity. The parameters  $\alpha \in (0, 2]$  and  $\beta \in [-1, +1]$  describe the robustness and the asymmetry of the distribution. The distributions of differenced series,  $P(\Delta_m I)$ , with  $\Delta_m I_n = I_{n+m} - I_n$ , fit to the symmetrical Lévy distributions:

$$P(\Delta_1 I) = P_{\text{st}}(0.7, 0), \quad P(\Delta_2 I) = P_{\text{st}}(0.5, 0). \quad (13)$$

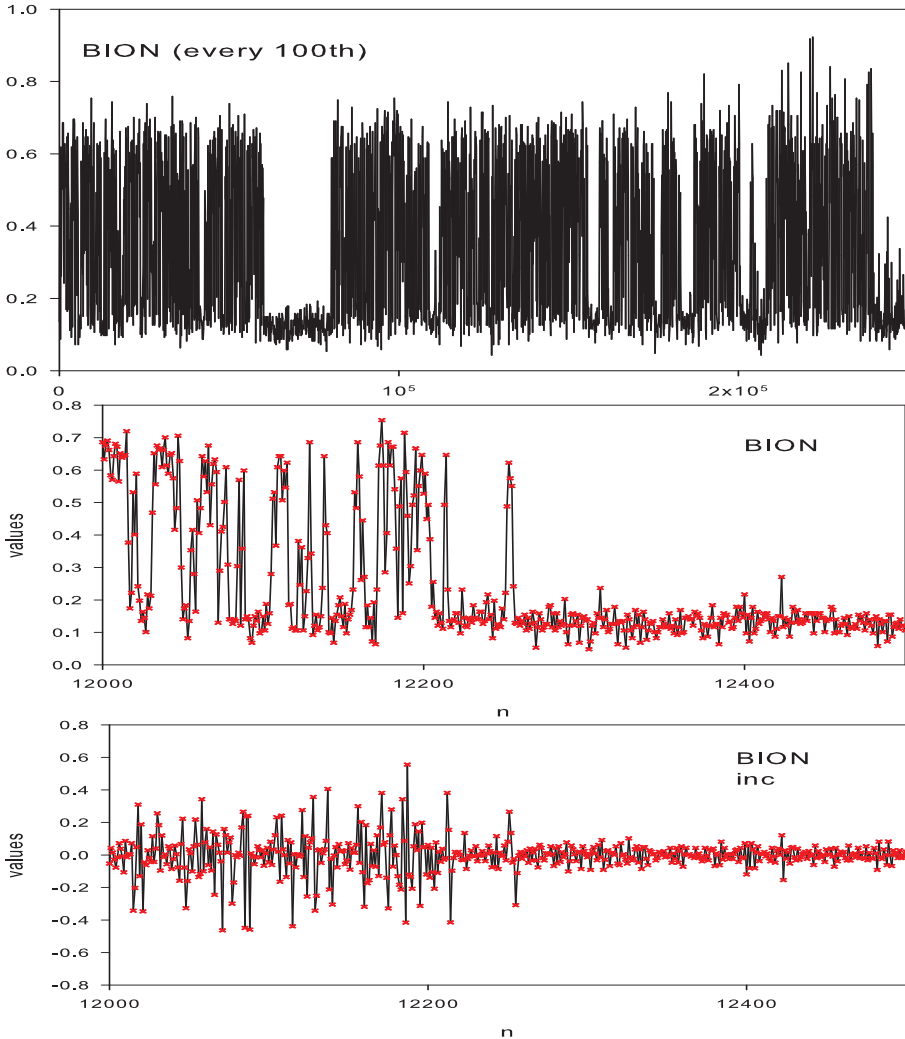


Fig. 8. The time dependence in BION series measured with resolution 0.1 msec (upper) and details of this dependence in the signal (middle) and in its increments (bottom). The lower values describe currents for the closed channel whereas the higher values correspond to currents when the channel is open.

The fits, obtained by the Nolan’s program STABLE [30], are shown in Fig. 9. Note that (i) for  $\alpha$ -stable distributions all moments higher than first are divergent (when  $1 < \alpha < 2$  the first moment is divergent also), therefore the standard definitions of variance, skewness, kurtosis do not hold; (ii) the differentiation removes the trends and non-stationarities from the signal — the resulting distributions are monomodal and symmetrical.

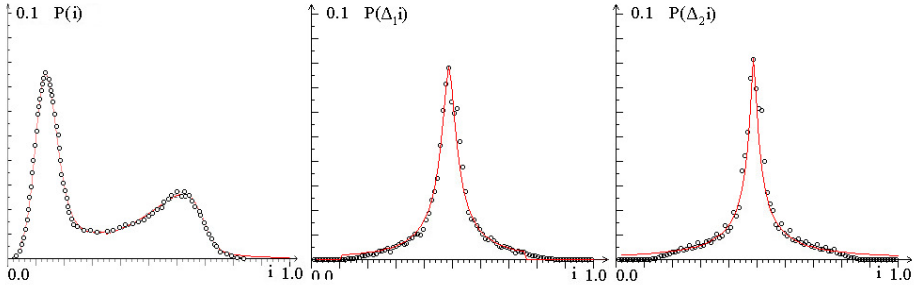


Fig. 9. Distributions (normalized histograms)  $P(i(t))$  of the series BION (circles), and corresponding fits (smooth, red curves, *cf.* text). (a) original signal, (b)–(c) — differenced series.

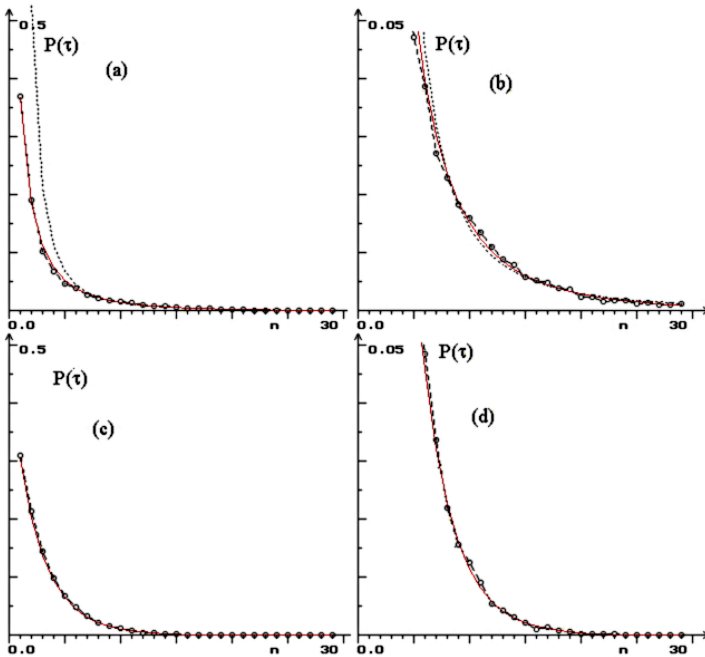


Fig. 10. Distributions (normalized histograms)  $P(\tau)$  of the series BION (circles) and fits: red — stretched exponential, cyan — algebraic. (a),(b): closed, (c),(d): open states.

Frequently used characteristics of currents through biological channels are so-called dwell times  $\tau$  (their distributions and average values) in a given channel state. Tail properties of BIO closed- and open-channel dwell times  $\tau$  were determined in [27]. The tails decrease according to power laws  $\tau^{-D}$  with the exponents  $D = 1.25 \pm 0.03$  for closed and  $D = 4.16 \pm 0.17$  for open channel. According to [28] the distribution of open channel dwell times

is exponential,  $P(\tau) \sim \exp(-\lambda\tau)$  with  $\lambda = 1.20 \pm 0.08 \text{ ms}^{-1}$ . Note that both the values and the distributions of dwell-times depend on the choice of threshold dividing the currents into “open” (high) and “closed” (low) ones. Taking threshold at the median of the distribution  $P(I)$  we found that  $P(\tau)$  fits well to stretched exponentials  $3.65 \exp\{-(\tau/0.011 \text{ ms})^{0.378}\}$  for closed, and  $0.49 \exp\{-(\tau/0.23 \text{ ms})^{0.90}\}$  for open channel (with about 5% error in these coefficients). Algebraic fits are worse. The results are shown in Fig. 10. The corresponding average dwell-times  $\langle\tau\rangle$  are  $5.93\delta t$  for closed (low-current) and  $3.31\delta t$  for open (high-current) states. The values of  $\langle\tau\rangle$  depend even more strongly on the choice of threshold and on  $\delta t$ .

5.2. Multifractal analysis of the BION signal

The length of the signal provides enough points to calculate the partition functions up to the scale of about  $n = 30\,000$ , see Fig. 11. It is evident that these partition functions depend on the scale. The scaling changes rapidly at about  $\log n \approx 4$  in both BION and integrated BION signals. However, this switch is evident only if  $q < -1.3$ , so, in the region which is numerically unstable. For positive  $qs$  the partition functions presents smooth behavior. Furthermore, the partition functions of the integrated

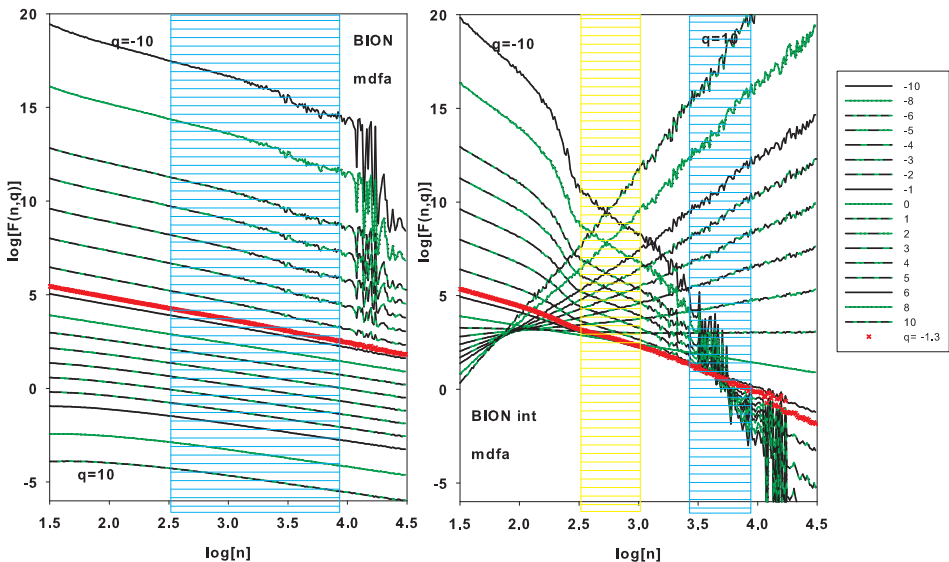


Fig. 11. Partition functions for BION series (left) and integrated BION series (right). Shaded rectangles point at scaling intervals used in analysis. The scaling features of the partition function of increments of BION are similar to the direct signal features.

signal exhibit additional differences in the scaling when  $\log n$  is about 2.3. Notice that this change is also evident only if  $q < -1.3$ . Therefore, we cannot conjecture if any of these changes is signs of some switch in mechanisms producing currents in the observed ion channel.

In Fig. 12 the multifractal spectra are presented when the scaling is performed in  $2.5 < \log n < 4$  region in the case of BION and increments of BION. In the case of integrated BION signal the two intervals:  $2.5 < \log n < 3$  (mid) and  $3.3 < \log n < 3.8$  (large) are used.

The conclusion of the previous section indicates (BION as an uncorrelated Lévy motion) that a two-point multifractal spectrum at  $(0,0)$  and  $(1/1.58 \approx 0.63, 0)$  should be received for the BION integrated signal. However, both spectra in Fig. 12, left top and left bottom are different from expected ones. Moreover, application of values of  $\tau(2)$  directly leads to  $H$  value close to 0 for BION. This suggests that LRD is not present among increments of BION. In the case of BION integrated  $H$  is close 1 what indicates a deterministic like correlations in BION.

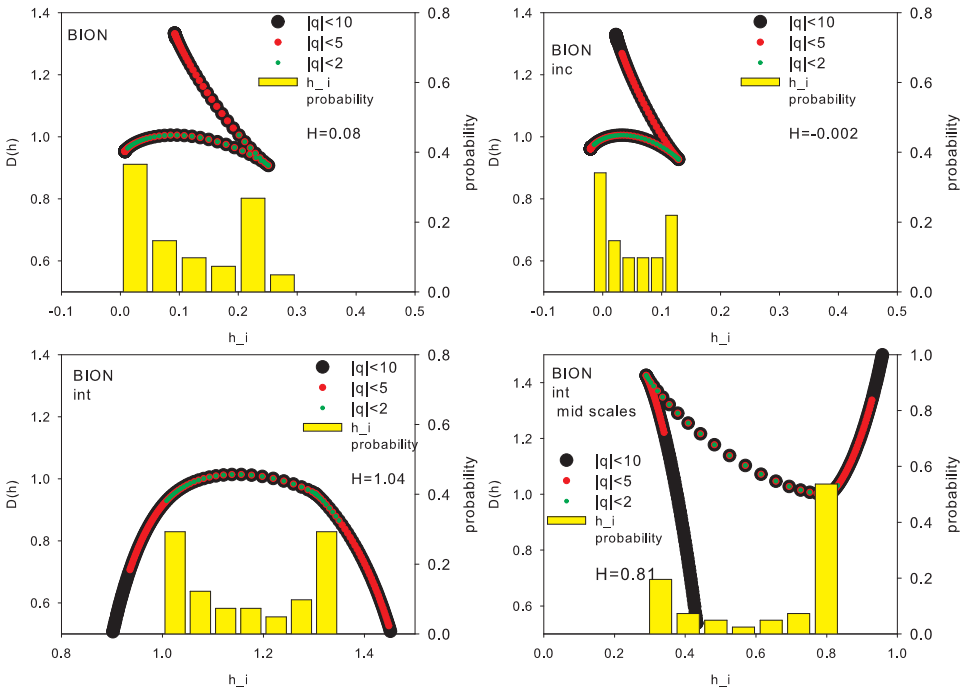


Fig. 12. Results of the multifractal analysis for BION, increments of BION and integrated BION.

Analysis of shuffled data, according to [5], provides a simple and efficient test for the presence of correlations. It appears that the multifractal spectra of the BION series shuffled at random are identical to  $fGn_{0.5}$ . Namely, the shuffled BION signal provides a very sharp spectrum at a point  $(0, 1)$  (with  $\Pr(h_{\text{acc}} = 0) = 1$  for  $|q| < 10$ ). For the integrated signal, the multifractal spectrum appears at the point  $(0.5, 1)$  (with  $\Pr(h_{\text{acc}} = 0.5) = 1$  for  $|q| < 3$ ).

The BION signal is a bimodal one with rather fixed dwell-times, so one can think whether its multifractal properties are similar to properties received from a *on-off* process with exponentially distributed *on* and *off* periods. Tests were performed to check whether where the random on-off signals perturbed by  $fGn_H$  gave multifractal indices similar to BION. However, independently of  $H$ , the multifractal spectra received were of  $fGn_{0.5}$ -type. Hence the dynamics of the switches is not the source for the observed multifractality of BION.

Thorough observations of plots in Fig. 12 reveals that multifractality of the BION signal can be described by two spectrum accumulation points:  $h'_{\text{acc}} \approx 0.03$  and  $h'_{\text{acc}} \approx 0.25$ , both attributed with  $D \gg 0$ . The spectrum of the integrated signal obtained in large scales gives also the two accumulation points which are located at about 1 and 1.35. Notice that these values are close to the exponent received from the ordinary power-spectrum analysis  $B = 1.1 \pm 0.1$ . Therefore, the multifractal features of BION can be considered as similar to results received when two anticorrelated fBm signals were discussed. If our observation is true then, following the conjecture (10), on the large scales  $H = -\tau(-2) - 1 \approx 0.48$  describes the larger self-similarity exponent of the two processes which form the BION signal. The justification for the appearance of such a mixture can be easily found in the biology of ionic currents — diffusion of potassium ions regulated strongly by both the channel shape and the electrostatic forces.

The interval where the different scaling in the integrated BION signal is observed (namely, mid scales) provides a rather distinct description to the BION series. The presence of a strong accumulation point at  $h = 0.8$  indicates that BION itself seems to be dominated by a persistent noise. Since the BION signal is long enough we were able to investigate this property in detail by studying multifractal properties in parts of the BION signal separately. We divide the series into five parts: (a), . . . , (e), consisting of subsequent 50 000 points each. The results are collected in Table I.

It appears that  $h_{\text{acc}} \approx 0.80$  is found in each part of  $\text{BION}^{\text{int}}$ , and, moreover, the same value is found for  $H$  calculated from  $\tau(2)$  what shows that at scales of hundreds of observation step, here 0.1 msec the persistent correlations are present among the BION data. On the other hand, the value  $H = 0.80$  can be also thought as closely related to the exponent which describes the decay of tails of the distribution fit to  $\alpha$ -stable distribution. This

similarity would rather indicate that LRD is not present in the BION signal. However, since the value of the second spectrum accumulation point is less fixed or even the second point is absent, then the direct conclusion is not clear. Having in mind that this property is not observed on large scales, therefore the property has transient character only. This property can be an evidence of either the presence of non-Gaussian distributions or persistency among BION data. From Table I one can read also about multifractal features of the parts of the BION signal itself. The results are similar to those obtained for the whole signal with the exception for the value of the self-similarity parameter  $H$  of the contributing process — the short data analysis shows at  $H = 0.30$ .

TABLE I

Results of the multifractal analysis applied to fragments of the BION series.

Part name	BION: $2 < \log(n) < 3.11$		BION <sup>int</sup> : $2.4 < \log(n) < 3.0$	
	$h_{\text{acc}}$	$H$ from $\tau(2)$ $H$ from $\tau(-2)$	$h_{\text{acc}}$	$H$ from $\tau(2)$
(a)	0.03 0.40	0.05 0.55	0.80 1.09	0.80
(b)	0.02 ... 0.08 uniform	0.05 0.18	0.80 0.36	0.80
(c)	0.04 0.26	0.04 0.36	0.77 ... 0.81 uniform	0.77
(d)	0.03 0.16	0.05 0.26	0.85 0.26	0.85
(e)	0.04 ... 0.08 uniform	0.05 0.17	0.83 0.61	0.83

## 6. Conclusions

Multifractal analysis needs a special care to avoid possible traps. Therefore much attention has to be put to proceed. The method of estimation of multifractality proposed here arises from the straightforward relationship between LRD and fBm $_H$ .

Our results show that the multifractal analysis of long series is able to detect the presence of two different signals. The fact that the currents through biological nano-channels correspond to two different states (open and closed) of the channel, is now well-known. However, the multifractal

analysis was able to say more about the properties of this mixture — at least that both signals are antipersistent. Features such as non-markovianity, long tails of dwell-time distributions fitting to stretched exponential functions, non-Gaussian long-tailed current distributions, persistence and multifractal spectra suggest strongly that the analyzed series is self-similar (direct proof would need the measurements on a few different time-scales), and that the underlying physical processes may have chaotic components, leading to anomalous kinetics. It is well-known that due to the narrowness of the biological channels, the ions move collectively in a single file [31], what implies the subdiffusional character of the transport.

The results presented in Fig. 9 and Fig. 10 show that these distributions are non-classical, *i.e.*, non-exponential, long-tailed ones contrary to popular beliefs expressed in the literature. As we mentioned earlier, a linear combination of sufficient number of appropriately chosen functions is able to reproduce any other function, especially when that function contains experimental errors. However, without any good physical reason for choosing both such functions and distributions of their weights (*i.e.*, when a number of functions entering into the combination is greater than two — three) such a procedure gives little insight into the properties and mechanisms of the processes underlying the examined data.

It was found earlier for BION series [28] that the Hurst exponent  $H = 0.84 \pm 0.08$ , *i.e.*, the fractal dimension  $D = 2 - H = 1.16 \pm 0.08$ . This led to the conclusion “that the transport of ions through a single-membrane channel is Gaussian, *i.e.*, the ionic current process finite-dimensional distributions are Gaussian. Because the self-similarity index  $H \neq 1/2$ , we claim that the process can be identified with a fractional Brownian motion (fBm)”. However, this result seems to be in contradiction with the value of the power spectrum exponent  $B = 1.1 \pm 0.1$  [25,26] which was also detected by multifractal tools. The possible persistence was found to be related to the transient scaling property, and therefore could lead to the misleading interpretation.

D.M. thanks the Polish Ministry of Science and Higher Education — PB: 1921/B/H03/2008/34 — for the financial support. Authors are grateful to Dr. Marcei Krogulec for his careful reading of the manuscript.

## Appendix A

Local slopes of the partition function  $F_{\text{fBm}_{0.2}}(n, q)$  calculated for a sample path of  $\text{fBm}_{0.2}$  are analyzed as follows. For fixed  $q$  the best linear fit for the subsequent 30 points of  $\log F_{\text{fBm}_{0.2}}(n, q)$  *vs.*  $\log n$  plot was found. Then, the starting point along the partition function was moved. This way a

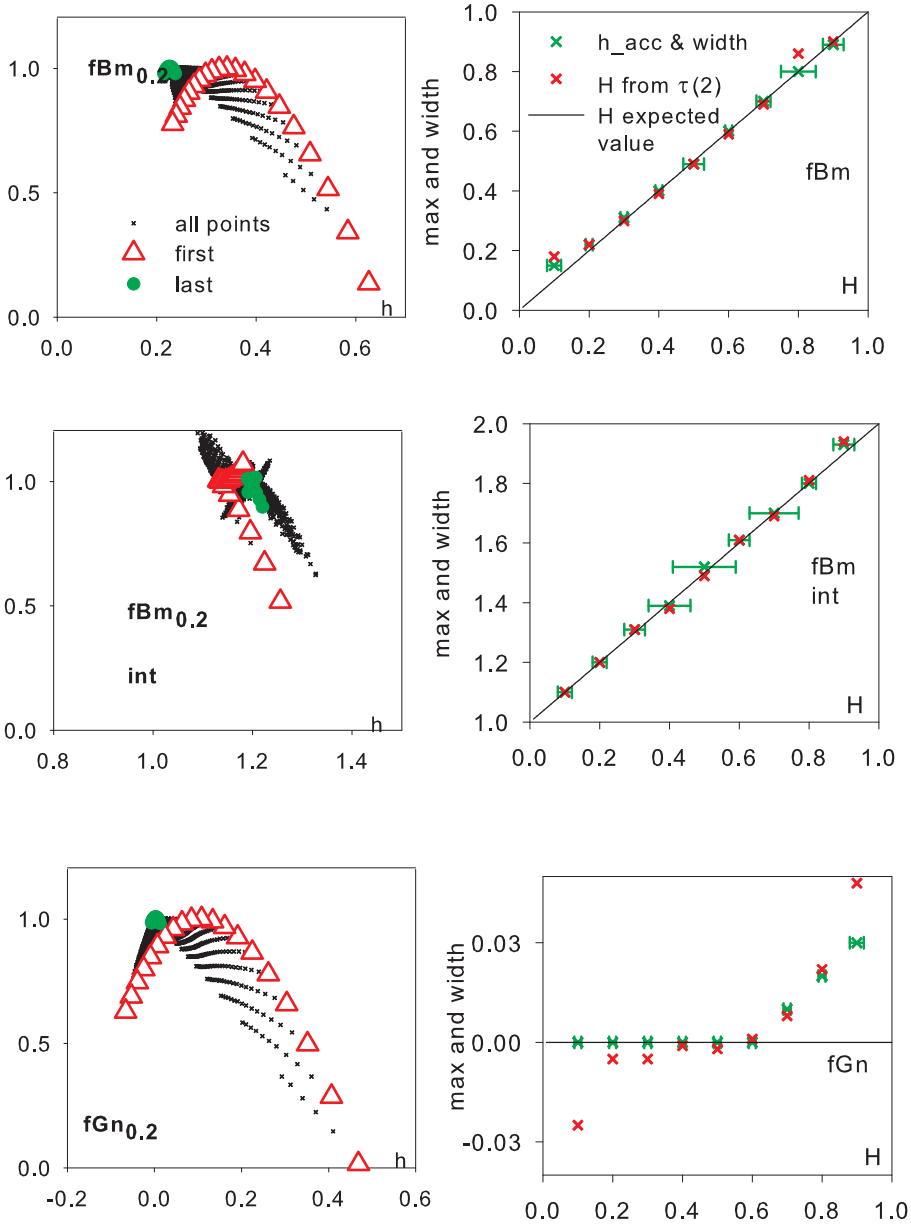


Fig. 13. Left column: Multifractal spectra received for different scaling intervals for a sample path of  $fBm_{0.2}$ : from fine scales  $20 < n < 50$  to large scales  $2500 < n < 5000$ . Right column: Self-similarity exponent  $H$  found for different  $fBm_H$  following the proposed protocol, for  $300 < n < 3000$  (namely, large scales):  $h_{acc}$  together with the spectra widths, and  $H$  from (9).

collection of possible approximations to  $\tau(q)$  is received. The corresponding multifractal spectra are shown in Fig. 13, left column. Curves labeled *first* (red plots) describe scales  $1.3 < \log n < 1.7$ . Plots labeled *last* correspond to scales of  $3.4 < \log n < 3.7$ . Remembering that the spectra should appear in the points  $(0.2, 1)$ ,  $(1.2, 1)$   $(0, 1)$  for  $fBm_{0.2}$ ,  $fBm_{0.2}^{int}$ ,  $fGn_{0.2}$  respectively, we see that using the MDFA method the proper values might be received only in large scales (see [6] for discussion).

In the case of  $fBm_H$  that crossover property is caused only by deficiency of the method. Hence, the MDFA method can be validated through its representation of a point spectrum of  $fBm_H$  and signals related to a given  $fBm_H$  such as  $fBm_H^{int}$  and  $fGn_H$ . In particular, the method's accuracy was assessed by testing: (i) the distance between the expected value and the value at which the maximum of a multifractal spectrum is attained, and (ii) the width of the multifractal spectrum.

### Appendix B

The other problems with multifractal results classification are related to the shapes of the multifractal spectra found numerically — compare, *e.g.*, shapes of spectra received for  $fBm_{0.2}^{int}$ . It appears that the Legendre transform (6) provides a convenient way to encode the scaling exponent function if  $\tau(q)$  is strictly convex. It means that not only the first derivative of  $\tau$  is important, as it provides the  $h$  values, but also  $h(q)$  has to be a strictly monotonic function [33]. However, it happens often that  $\tau(q)$  is not a convex function, so that the corresponding multifractal spectrum is a multivalued function.

Fortunately, the multifractal spectrum shapes can be considered as systematic modifications of the parabola-like shape, see Fig. 14 as the example. We believe that these modifications are mainly caused by numerics. Namely,

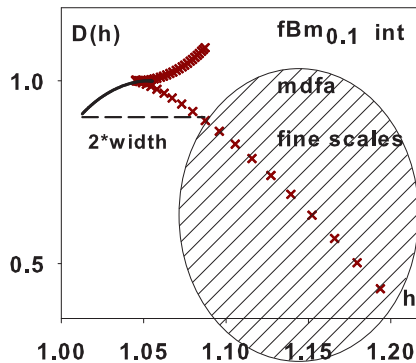


Fig. 14. Illustration of a multifractal spectrum analysis if the spectrum is a non-symmetrical and multivalued function.

when a partition function is calculated for  $q < 0$ , one takes into account the influence of small fluctuations which practically means dealing with numbers close to zero. Most of numerical methods do not cope properly with this problem. In the case of MDFA a nonsymmetric parabola was often obtained where the right wing of a spectrum (*i.e.*, a part which corresponds to negative  $qs$ ) is significantly larger than the left one. The multivalued spectrum is always due to the switch in the convexity of  $\tau(q)$ .

### Appendix C

In the case of self-similar signals with self-similarity exponent  $H$ , searching for the maximum of a multifractal spectrum, we expect that a set of  $\{h_i\}$ :

$$h_i = \frac{\Delta\tau(q_i)}{\Delta q} = \frac{[\tau(q_i + \Delta q), -\tau(q_i)]}{\Delta q}, \quad (14)$$

where  $q_i = q_0 + i\Delta q$  and  $\Delta q > 0$  is small enough should consist of values which are scattered close to  $H$ . Moreover  $h_i = H$  should have the highest count in the set  $\{h_i\}$ . We will call  $h_i$  with the highest count a *spectrum accumulation point*. However, each local peak in  $\{h_i\}$  will be called a *spectrum accumulation point*, too, and denoted  $h_{\text{acc}}$ . It is expected that in the case of  $\text{fBm}_H$ ,  $\text{fBm}_H^{\text{int}}$  and  $\text{fGn}_H$  signals, a single spectrum accumulation point is obtained and its value coincides with the maximum in a multifractal spectrum. Thus, a spectrum accumulation point for the  $\text{fBm}_H$  series is  $H$ , for  $\text{fBm}_H^{\text{int}}$ , is  $1 + H$  and in case of  $\text{fGn}_H$  is zero.

It appears that the values of spectrum accumulation points could depend on the interval of  $q$  for which the partition function is calculated [32]. If  $|q|$  is large then both negative ( $q < 0$ ) and positive ( $q > 0$ ) parts of  $\tau(q)$  can be fitted separately by different linear functions. Therefore formula (14) provides two spectrum accumulation points which are located at the limits of the spectrum rather than at its maximum, see [7] for details. The values of these accumulation points are weakly dependent on the expected value and they vary from sample to sample. However, when  $|q|$ -interval becomes narrower, these two limiting accumulation points disappear, and a single  $h_{\text{acc}}$  emerges.

### REFERENCES

- [1] G. Rangarajan, M. Ding (Eds.), *Processes with Long-Range Correlations. Theory and Applications, Lect. Notes Phys.* **621** 2003.
- [2] B. Lashermes, P. Abry, P. Chainais, *New Insights into the Estimation of Scaling Exponents, Int. J. Wavelets Multiresolut. Inf. Process.* **2(4)**, 497 (2004).
- [3] D. Veitch, N. Hohn, P. Abry, *Comp. Networks* **48**, 293 (2005).

- [4] S. Stoev, M.S. Taqqu, Ch. Park, J.S. Maroon, *Comp. Networks* **48**, 423 (2005).
- [5] J.W. Kantelhardt, [arXiv:0804.0747v1](https://arxiv.org/abs/0804.0747v1) [physics.data-an].
- [6] D. Makowiec, A. Dudkowska, R. Gałaska, A. Rynkiewicz, *Physica A* **388**, 3486 (2009).
- [7] D. Makowiec, A. Dudkowska, R. Gałaska, A. Rynkiewicz, J. Wdowczyk-Szulc, *Acta Phys. Pol. B* **40**, 1521 (2009).
- [8] C.O. Tan, M.A. Cohen, D.L. Eckberg, J.A. Taylor, *J. Physiol.* **587(15)**, 3929 (2009).
- [9] R.H. Riedi, *Multifractal Processes in Long-range Dependence: Theory and Applications* P. Doukhan, G. Oppenheim, M.S. Taqqu (Eds.), Cambridge MA, Birkhäuser, 2001, pp. 625–716.
- [10] D. Cox, *Long-range Dependence: A Review in Statistics: An Appraisal*, H.A. David, H.T. David (Eds.), The Iowa State University Press, 1984, pp. 55–74.
- [11] T. Karagiannis, M. Molle, M. Faloutsos, *IEEE Internet Computing* **8**, 57 (2004).
- [12] E. Bacry, J.F. Muzy, A. Arnedo, *J. Stat. Phys.* **70**, 635 (1993); J.F. Muzy, E. Bacry, A. Arnedo, *Phys. Rev.* **E47**, 875 (1993).
- [13] J.W. Kantelhardt, S.A. Zschiegner, E. Koscielny-Bunde, S. Havlin, A. Bunde, H. E. Stanley, *Physica A* **316**, 87 (2002).
- [14] B. Lashermes, S.G. Roux, P. Abry, S. Jaffard, *Eur. Phys. J.* **B61**, 201 (2008).
- [15] P. Oświęcimka, J. Kwapiień, S. Drożdż, *Phys. Rev.* **E74**, 016103 (2006).
- [16] A.L. Goldberger, L.A.N. Amaral, L. Glass, J.M. Hausdorff, P.Ch. Ivanov, R.G. Mark, J.E. Mietus, G.B. Moody, C.-K. Peng, H.E. Stanley, *Circulation* **101(23)**, e215 (2000) [Circulation Electronic Pages <http://circ.ahajournals.org/cgi/content/full/101/23/e215>].
- [17] J. Barral, J. Levy Vehel, *Electronic J. Probability* **9**, 508 (2004).
- [18] K. Hu, P.Ch. Ivanov, Z. Chen, P. Carpena, H.E. Stanley, *Phys. Rev.* **E64**, 011114 (2001).
- [19] S. Drożdż, J. Kwapiień, P. Oświęcimka, R. Rak, *EPL* **88**, 60003 (2009) [[arXiv:0907.2866v1](https://arxiv.org/abs/0907.2866v1) [physics.data-an]].
- [20] J. Conove, <http://www.johncon.com/>, Copyright 1994–2005, John Conover, All Rights Reserved.
- [21] D.A. Doyle *Science* **280**, 69 (1998).
- [22] G. Yellen, *Nature* **419**, 35 (2002).
- [23] F. Gorczynska, P.L. Huddie, B.A. Miller, I.R. Mellor, H. Vais, R.L. Ramsey, P.N.R. Usherwood, *Pflügers Arch. — Eur. J. Physiol.* **432**, 597 (1996).
- [24] A. Fuliński, Z. Grzywna, I. Mellor, Z. Siwy, P.N.R. Usherwood, *Phys. Rev.* **E58**, 919 (1998).
- [25] Z. Siwy, A. Fuliński, *Phys. Rev. Lett* **89**, 158101 (2002).
- [26] Z. Siwy, A. Fuliński, *1/f Noise in Ion Transport Through Nanopores: Origins and Mechanism* in: *Unsolved Problems of Noise and Fluctuations: UpoN 2002*, S.M. Bezrukov (Ed.), *AIP Conf. Proc.* **665**, 273 (2003).

- [27] S. Mercik, K. Weron, Z. Siwy, *Phys. Rev.* **E60**, 7343 (1999).
- [28] S. Mercik, K. Weron, *Phys. Rev.* **E63**, 051910 (2001).
- [29] Z. Siwy, S. Mercik, K. Weron, M. Ausloos, *Physica A* **297**, 79 (2001).
- [30] The program STABLE is available from J.P. Nolan's website:  
<http://academic2.american.edu/~jpnolan>; cf. also: J.P. Nolan, *Stable Distributions — Models for Heavy Tailed Data*,  
<http://academic2.american.edu/~jpnolan>
- [31] S. Bernèche, B. Roux, *Nature* **414**, 73 (2001).
- [32] P. Abry, S. Jaffard, B. Lashermes, *Optic East, Wavelet Applications in Industrial Applications II* vol. 5607, p. 103, Philadelphia, USA, 2004.
- [33] R.K.P. Zia, E.F. Redish, S.R. Mckay, [arXiv:0806.1147v2](https://arxiv.org/abs/0806.1147v2) [physics.ed-ph].